Photoinduced metastable state with modulated Josephson coupling strengths in $Pr_{0.88}LaCe_{0.12}CuO_4$

S. J. Zhang,[1] Z. X. Wang,[1] D. Wu,[1] Q. M. Liu,[1] L. Y. Shi,[1] T. Lin,[1] S. L. Li,[2,3] P. C. Dai,[4] T. Dong,[1] and N. L. Wang[1,3,*]

[1]*International Center for Quantum Materials, School of Physics, Peking University, Beijing 100871, China*

[2]*Institute of Physics, Chinese Academy of Sciences, Beijing 100190, China*

[3]*Collaborative Innovation Center of Quantum Matter, Beijing 100871, China*

[4]*Department of Physics and Astronomy, Rice University, Houston, Texas 77005, USA*

(Received 26 August 2018; revised manuscript received 22 November 2018; published 12 December 2018)

We report an intense near-infrared pump, c-axis terahertz probe measurement on an electron-doped cuprate superconductor $Pr_{0.88}LaCe_{0.12}CuO_4$ with $T_c = 22$ K. The major effect of the intense pump is to induce a splitting of Josephson plasma edge below T_c, similar to the observation on hole-doped cuprate $La_{1.905}Ba_{0.095}CuO_4$ in a superconducting state. The photoexcitation induced spectral change does not exhibit significant decay up to the longest measured time delay 210 ps. The result suggests that the intense near-infrared pump drives the system from a superconducting state with a uniform Josephson coupling to a metastable superconducting phase with modulated Josephson coupling strengths below T_c.

DOI: 10.1103/PhysRevB.98.224507

Electron-doped high-T_c superconducting cuprates (HTSCs), as a family of superconducting copper oxides, are often investigated by comparing with hole-doped ones [1,2]. Electron-doped HTSCs can be realized only in specific "214" T' structure, e.g., Ce-doped Nd_2CuO_4 [1], or related rare-earth element-based compounds such as $Pr_{2-x}Ce_xCuO_4$, $Pr_{1-x}LaCe_xCuO_4$, etc. Compared with hole-doped $La_{1-x}Ba_xCuO_4$ with K_2NiF_4 structure (T structure), the out-of-plane oxygen shifts from the apical position to the fixed position $(0, 1/2, 1/4)$. This shift alters the coordination of both Cu and rare-earth element (Ln) atoms. Copper becomes strictly square-planar coordinated with no apical oxygens. A comparison between T' and T structures is shown in Fig. 1(a). Multiple other aspects have already been verified exhibiting both similarities and differences between those two structure-type compounds [3].

Time-resolved spectroscopy can give unique insight into the dynamical properties of the elementary excitations in quantum materials [4]. Up to now, ultrafast pump-probe measurements performed on electron-doped HTSCs were dedicated to disentangle complex degrees of freedom in the system [5–10], in which the fluence of pump pulses is always quite small and regarded as weak external perturbations for material systems. In single-color pump-probe experiments on electron-doped HTSCs [5–9], near-infrared (NIR) pump pulses with the fluence below 10 $\mu J/cm^2$ were expected to suppress/destroy superconductivity by breaking Cooper pairs into quasiparticles. Using some effective phenomenological models such as the Rothwarf-Taylor model [11], the subsequent decay procedure of those quasiparticles may disclose the complex interplay among electrons, lattice, and spin dynamics. In NIR/terahertz (THz) pump-THz probe measurements in the ab plane of $Pr_{1.85}Ce_{0.15}CuO_{4-\delta}$ [10], the depletion and the recovery of the superconducting state after being excited by pump pulses were observed in the pump-induced change of conductivity.

Distinguished from weak pump pulses expected to excite quasiparticles from an occupied state to an unoccupied one, intense pump pulses tend to induce a phase transition and drive a material system to a phase inaccessible for traditional physical parameters such as temperature and pressure [12–14], which provide unique opportunities to manipulate different orders in complex material systems. A surprising finding is that intense midinfrared ultrafast excitation can drive a nonsuperconducting hole-doped HTSC into a phase with a Josephson-plasmon-like edge in the c-axis optical spectra, which was observed in a stripe-ordered cuprate at 10 K whose T_c is less than 2 K [15], then in underdoped $YBa_2Cu_3O_{6.5}$ even above room temperature [16,17]. Later on, it was found that intense NIR pulses can also induce a phase change in $La_{2-x}Ba_xCuO_4$ systems [18–20].

Here we report photoexcited c-axis dynamics in an electron-doped cuprate $Pr_{0.88}LaCe_{0.12}CuO_4$ (PLCCO) with $T_c = 22$ K after the excitation of intense NIR pump at 1.28 μm with polarization of the $\mathbf{E} \parallel c$ axis. We observe a photoexcitation induced split of the Josephson plasmon edge (JPE) in the superconducting state. Remarkably, no significant decay is observed up to the longest measurement time delay 210 ps after excitation. The observation indicates clearly that the intense pump with energy much higher than the superconducting pairing energy drives the system from a superconducting state with a uniform Josephson coupling to a metastable superconducting phase with modulated Josephson coupling strengths. The measurement results may shed light in understanding the photoinduced phase transition phenomena in cuprates and other nonequilibrium experiments.

Single crystals of PLCCO were grown using the traveling-solvent floating-zone technique. A post-annealing process was conducted to remove excess oxygen and induce superconductivity [21]. The temperature-dependent magnetic susceptibility was measured by a Quantum Design

*nlwang@pku.edu.cn

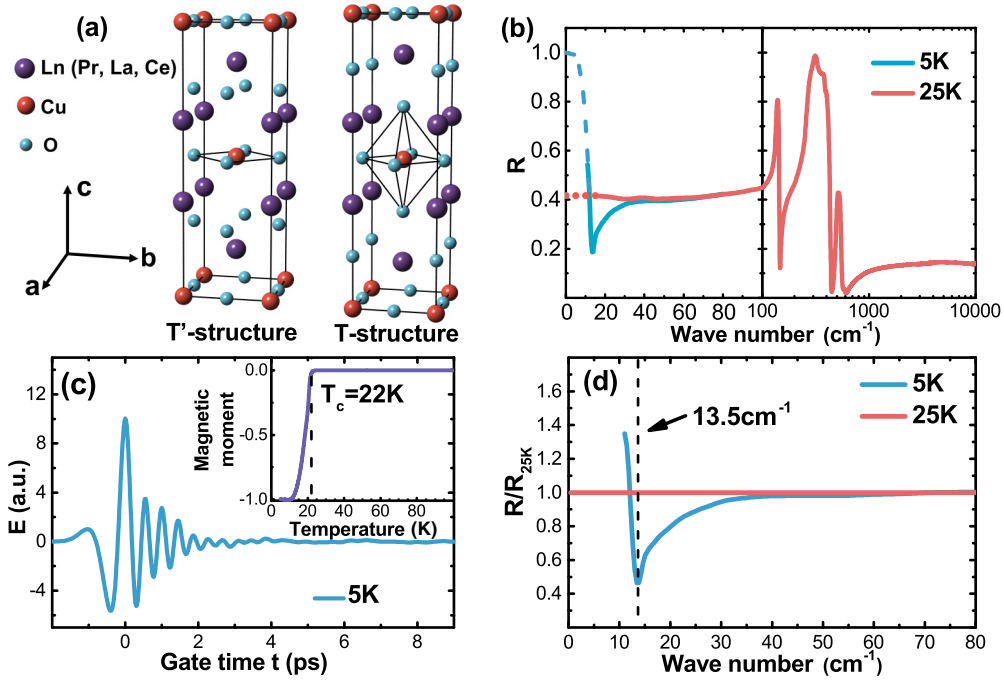

FIG. 1. Sample structure and characterization. (a) A comparison between T' and T structures. The T' structure is characterized by a lack of apical oxygen compared with T-structured hole-doped HTSC. (b) The broadband reflectivity spectra at 25 and 5 K are acquired by combining the measurements of FTIR and THz time-domain spectrometers. Solid lines indicate the experimental data and dash/dot lines indicate low-frequency extrapolations (details can be found in the main text). (c) Inset: a sharp superconducting transition at $T_c = 22$ K is determined by temperature-dependent magnetic susceptibility measurement. Main panel: the reflected THz electric field of PLCCO along c-axis at 5 K is characterized by a THz time-domain spectrometer. (d) Reflected spectra at 5 K (below T_c) are normalized to spectra at 25 K (above T_c). A very sharp JPE develops near 13.5 cm^{-1} at 5 K, which is indicated by a dashed line.

physical property measurement system, as shown in the inset of Fig. 1(c).

In order to get the photoexcited charge dynamical properties, the optical constants in the equilibrium state have to be known prior to the photoexcition measurement. Those optical constants can be obtained through Kramers-Kronig transformation of broadband reflectivity. A finely polished ac plane of the crystal, which has a half-moon shape with a diameter of 4 mm, was used for optical measurements. The broadband c-axis optical reflectivity spectra of PLCCO were acquired by a combination of Fourier transform infrared spectrometers (FTIR) (Bruker 113v and Vertex 80v, ranging from 15 to 15 000 cm^{-1}) and a time-domain THz spectrometer (ranging from 10 to 80 cm^{-1}). A near normal incidence configuration and *in situ* gold overcoating technique were used to get reflectivity $R(\omega)$ in FTIR measurements. The equilibrium and photoexcitation induced change of c-axis reflectivity ranging from 0.3 to 2.4 THz were measured by a time-domain THz spectroscopy system, which is constructed based on an amplified Ti:sapphire laser system producing 800-nm, 35-fs pulses at a 1-kHz repetition rate. A THz probe beam is generated from 800-nm pulses on a (110) ZnTe crystal without any focalization, and the ZnTe is in size of 10 mm × 10 mm × 1 mm. Using a 30° off-axis parabolic mirror whose focal length is 54.45 mm, the spot size of THz probe beam at the sample position is focused into 0.63 mm, which was determined by a knife-edge method. The THz profile was detected via electro-optic sampling using a 1-mm-thick ZnTe. The 1.28-μm pump beam is generated by an optical parametric amplifier and focused into 1.2 mm at the sample position, which will provide nearly homogeneous excitation with sufficient pump fluence. Detailed experimental setup and measurement techniques are presented elsewhere [20,22].

HTSCs are highly anisotropic materials, in which conducting CuO_2 layers are usually separated by insulating block layers, leading to insulatorlike dc and optical responses along the c axis in the normal state. Reflectivity at 25 K, i.e., $R_{25K}(\omega)$, is very low and almost flat down to the lowest measurement frequency 15 cm^{-1} by our FTIR spectrometers, as shown in Fig. 1(b). At 5 K below T_c, we observed a strong downward curvature in the low-frequency range between 40 and 15 cm^{-1}, however the sharp upturn of the JPE was not observed due to the measurement limitation of FTIR. So, a THz time-domain spectrometer is used to determine the reflectivity below T_c, especially the Josephson plasmon edge. According to the definition $R(\omega) = |\tilde{r}(\omega)|^2 = |\tilde{E}_{\text{reflected}}(\omega)/\tilde{E}_{\text{incident}}(\omega)|^2$, the relative reflectivity ratio of different temperature $R_{5K}(\omega)/R_{25K}(\omega) = |\tilde{E}_{5K}(\omega)/\tilde{E}_{25K}(\omega)|^2$ can be acquired by measuring the strengths of reflected THz electric field $\tilde{E}_{5K}(\omega)$ and $\tilde{E}_{25K}(\omega)$ using a THz time-domain spectrometer. $R_{5K}(\omega)$ at lower frequencies can be acquired according to the ratios $R_{5K}(\omega)/R_{25K}(\omega)$. Figure 1(c) displays the reflected THz electric field $E(t)$ of PLCCO at 5 K in the time domain recorded by electric-optic sampling. The time zero $E(t = 0$ ps) is denoted as the peak position of $E(t)$, i.e., E_{peak}. Figure 1(d) shows the normalized reflected spectra

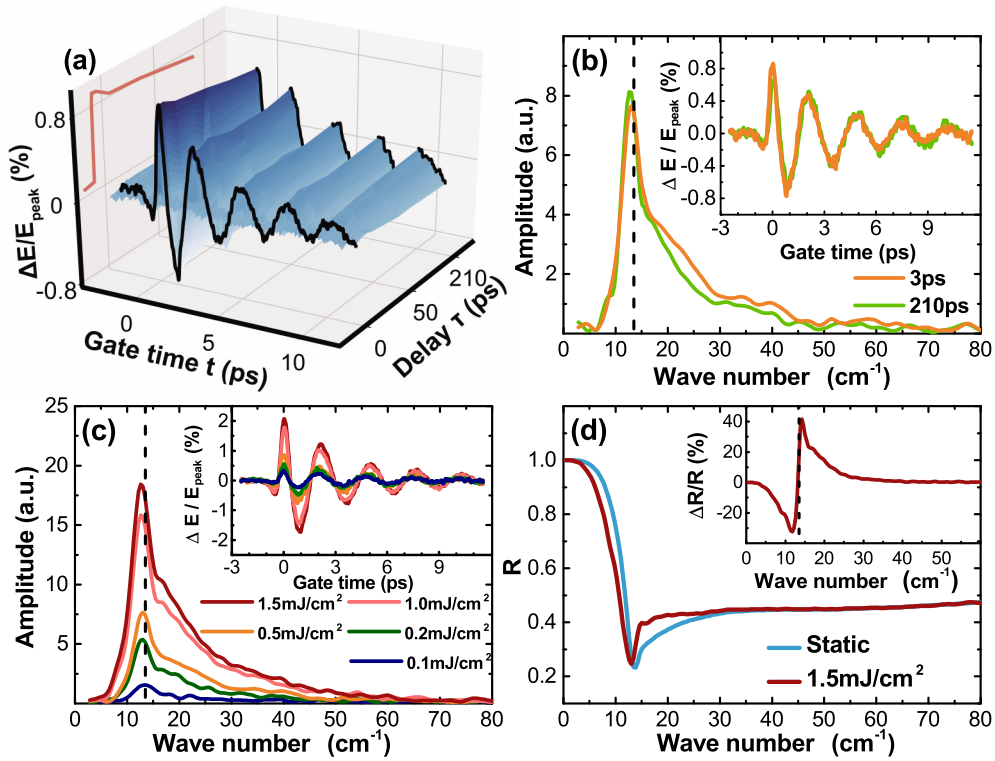

FIG. 2. Photoexcitation-induced changes at 5 K. (a) The relative change of the reflected THz electric field $\Delta E(t,\tau)/E_{\rm peak}$ at 5 K at different decay time τ after excited by 1.28 μm pulses at fluence of 0.5 mJ/cm^2. The red line shows the decay of $\Delta E(t=0\ {\rm ps},\tau)/E_{\rm peak}$. The black lines indicate $\Delta E(t,\tau=3\ {\rm ps})/E_{\rm peak}$ and $\Delta E(t,\tau=210\ {\rm ps})/E_{\rm peak}$. (b) Inset: the photoexcitation-induced relative change $\Delta E(t,\tau)/E_{\rm peak}$ in time domain at $\tau=3$ and 210 ps. Main panel: the Fourier transformed spectrum of $\Delta E(\omega,\tau)$. (c) Inset: fluence dependence of $\Delta E(t,\tau)/E_{\rm peak}$. Main panel: the Fourier transformed spectrum. (d) $R(\omega)$ before and after excitation by 1.5-mJ/cm^2 pulses. Inset shows the ratio of the reflectivity change relative to the static values. The penetration depth mismatch is not considered here.

below and above T_c, which affects us to see clear development of the JPE at 5 K. The broadband c-axis optical reflectivity spectra are presented in Fig. 1(b). The Kramers-Kronig transformation requires further extrapolation of $R(\omega)$ to zero frequency, in addition to the high-frequency extrapolation. At 5 K below T_c, the low frequency below 10 cm^{-1} was extrapolated using $1-R(\omega)_{5K}\propto\omega^4$. At 25 K, the low-frequency reflectivity $R_{25K}(\omega)$ below 15 cm^{-1} was extrapolated in a constant form as shown in Fig. 1(b) (red dots).

The low-frequency c-axis optical spectra are dominated by the infrared active phonons with little contribution from free carriers. In the normal state, reflectivity below 80 cm^{-1} (or 2.5 THz) is low and almost featureless, indicating an insulating response. However, when PLCCO goes into a superconducting state, a JPE develops in the c-axis reflectivity spectra and lies near 13.5 cm^{-1} at 5 K, which is caused by the Josephson tunneling effect of condensed superfluid carriers. Manifestation of such c-axis plasma edge is taken as an optical evidence for the occurrence of superconductivity. The reflectivity spectra are similar to those measured on $Nd_{1.85}Ce_{0.15}CuO_4$ [23]. In addition, the JPE has been observed in many hole-doped cuprates as well—some are higher than what is observed here (e.g., $YBa_2Cu_3O_{7-x}$ [24,25]), while the JPE in optimally doped $Bi_2Sr_2CaCu_2O_8$ [26] is smaller, occurring below the THz region generated by ZnTe crystal.

Figure 2(a) illustrates the relative changes of the reflected THz electric field $\Delta E(t,\tau)/E_{\rm peak}$ at 5 K at different decay time τ after excited by 1.28-μm pulses at fluence of 0.5 mJ/cm^2. We define time zero of the decay procedure $\tau=0$ ps at the position where $\Delta E(t=0\ {\rm ps},\tau)/E_{\rm peak}$ starts to change, so the state before $\tau=0$ ps is defined as static state. The red line shows the decay of $\Delta E(t=0\ {\rm ps},\tau)/E_{\rm peak}$. The black lines indicate the relative change of THz electric field at $\tau=3$ and 210 ps respectively, i.e., $\Delta E(t,\tau=3\ {\rm ps})/E_{\rm peak}$ and $\Delta E(t,\tau=210\ {\rm ps})/E_{\rm peak}$, which is also presented in the inset of Fig. 2(b) more clearly. Roughly a 0.8% maximum relative change is seen within 3 ps after excitation and clear oscillations can be seen in $\Delta E(t,\tau)/E_{\rm peak}$, which gives a peak slightly below 13.5 cm^{-1} in frequency domain $\Delta E(\omega,\tau)$ after Fourier transformation, as shown in the main panel of Fig. 2(b). The signal does not show significant decay up to the longest measured time delay of 210 ps. This pronounced peak in $\Delta E(\omega,\tau)$ suggests that photoexcitation-induced change occurs predominantly near the static JPE position. We also performed NIR pump THz probe measurements at different pump fluence as shown in Fig. 2(c). It can be seen that the pump-induced change gets more and more significant at increasing pump fluence. Figure 2(d) shows the reflectivity spectrum calculated from complex reflection coefficient [20] at $\tau=3$ ps after excited by 1.5-mJ/cm^2 pulses. The static reflectivity is also plotted for comparison. The main changes after excitation are the slight redshift of static JPE and the lifting of reflectivity above the static JPE position. Reflectivity spectra at $\tau=3$ ps merges into the static one above 30 cm^{-1}.

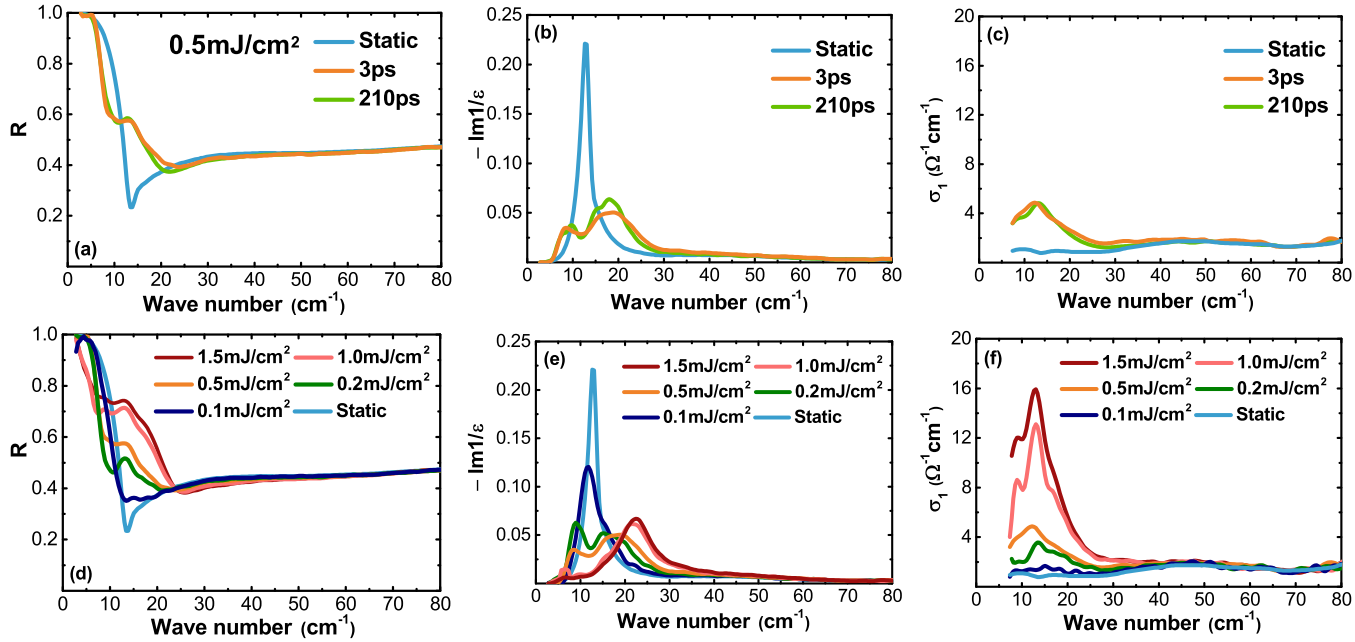

FIG. 3. Calculated optical constants from a multilayer model. Panels (a)–(c) show the temporal evolution of calculated $R(\omega)$, energy-loss function $\mathrm{Im}[-1/\varepsilon(\omega)]$, and real part of conductivity spectra $\sigma_1(\omega)$ after photoexcitations. No significant change can be found in the decay procedure. Panels (d)–(f) show the fluence dependence of photoexcitation induced values. The photoexitation induced change gets more and more significant as increasing pump fluence.

Those features can be more clearly observed in the ratio of reflectivity change over the static values, as shown in the inset of Fig. 2(d).

It deserves emphasizing that the NIR pump beam has much shorter penetration depth than the THz probe beam does due to their huge energy difference. The reflected probe field contains a mixed response of both pumped and unpumped portions of the compound. One has to disentangle those contributions in order to obtain the correct pump-induced change of optical properties. In literature, the pump-probe penetration depth mismatch was taken into account by using two different but related approaches, namely single layer and multilayer models [17,20]. We found that both approaches yield essentially the same results with a minor quantitative difference in our earlier work on $La_{1.905}Ba_{0.095}CuO_4$ [20].

In Fig. 3, a multilayer model is used for calculating the photoexcitation induced change of reflectivity $R(\omega)$, energy-loss function $\mathrm{Im}[-1/\varepsilon(\omega)]$, and the real part of conductivity spectra $\sigma_1(\omega)$, to eliminate the effects of penetration depths mismatch between 1.28-μm pump pulses and THz probe pulses (wavelengths range from 120 to 1000 μm) [20]. We first examine $R(\omega)$ at two representative time delays after excitation. At the maximum photoexcitation induced signal position, i.e., $\tau = 3$ ps [Fig. 3(a)], two edges can be seen in $R(\omega)$, which locate just below and above the static JPE position. They can be identified more clearly as peaks in $\mathrm{Im}[-1/\varepsilon(\omega)]$ as presented in Fig. 3(b). Compared with the static state with only one longitudinal Josephson plasmon mode, the photoexcitation induced effect is the splitting of the peak in $\mathrm{Im}[-1/\varepsilon(\omega)]$, which represents the emergence of two longitudinal Josephson plasmon modes with modulated Josephson coupling strengths. The presence of two longitudinal Josephson plasmon modes would result in the formation of a transverse Josephson plasmon mode, which can be seen as a peak in $\sigma_1(\omega)$ as shown in Fig. 3(c). This transverse Josephson plasmon mode can be regarded as an out-of-phase oscillation of the two individual longitudinal Josephson plasmon modes [27] and has been observed in many bilayer cuprate systems [28–31]. Nevertheless, it has never been observed in single layered cuprates in the equilibrium state. Similar effects can be also observed at $\tau = 210$ ps and there is no distinct difference between these two time delays, which indicates that PLCCO may have been driven into a metastable state by the pump pulses. We emphasize that the above results do not depend on the low-frequency extrapolation used in the Kramers-Kronig transformation at 25 K due to the sufficiently low energy scale achieved in our FTIR measurement. We actually tried a Hagen-Rubens extrapolation for the spectrum at 25 K and found that the calculated pump-induced optical constants are essentially the same.

Figures 3(d)–3(f) show the fluence dependence of photoexcitation induced change at $\tau = 3$ ps. When the pump fluence is quite small, e.g., 0.1 mJ/cm^2, only a slight redshift of static JPE and a lifting of reflectivity above the static JPE position can be observed in $R(\omega)$. With increasing the pump fluence, the static JPEs are suppressed to lower energy scale and a new edge above static JPE position with an increasingly higher energy scale can be observed as shown in Fig. 3(d). Figure 3(e) shows the corresponding energy-loss function. When the pump fluence is tuned from 0.1 to 0.5 mJ/cm^2, the separation of the two peaks in $\mathrm{Im}[-1/\varepsilon(\omega)]$ gets more and more pronounced. Meanwhile, the photoexcitation induced new longitudinal mode at higher energy gets more pronounced with increasing the pump fluence. When the fluence goes above 1 mJ/cm^2, the edge at lower frequency in reflectance $R(\omega)$ becomes less pronounced, but the edge at higher

frequency becomes more eminent. Then the peak feature in $\mathrm{Im}[-1/\varepsilon(\omega)]$ corresponding to the lower edge becomes almost invisible, which may result from the measurement limitation of THz pulses generated by ZnTe crysals. Meanwhile, the peak in $\sigma_1(\omega)$ gets more and more significant as shown in Fig. 3(f). The most prominent result of our experiments is the observation of photoinduced two long-lived longitudinal Josephson plasmon modes and a transverse plasmon mode. It suggests the development of two inequivalent Josephson couplings along the c axis.

The experimental result is highly nontrivial for two reasons. First, the photon energy of the NIR pump is much higher than the superconducting energy gap 2Δ; it is expected that the intense pump would break Cooper pairs and destroy superconductivity. However, this is not the case. The compound is still superconducting, nevertheless with modulated Josephson coupling strengths. Second, the NIR pump should excite quasiparticles from occupied state to unoccupied state far above the Fermi level, so after excitations one would normally expect to detect the nonequilibrium dynamics of those excited quasiparticles relaxing towards the equilibrium state via different quasiparticle-bosonic excitation interactions. This appears also not the case, or at most a minor effect. The true and dominant effect of intense pump is to drive the system to a new metastable state that does not exist before excitations.

Josephson coupling with multiple coupling strengths primarily comes from either the crystal structure with various kinds of Josephson junctions [28–31] or the external magnetic field induced effect [32,33]. Nevertheless, it seems impossible for the magnetic field component of a pump pulses with 35-fs pulse duration to induce long-lived Josephson vortices in alternate insulating layers and to last for more than 210 ps. Since the system goes to a new state in which the physical properties do not change appreciably with time delay, we have to consider a subtle structural phase transition induced by the intense pump. In fact, photoinduced structural phase transitions have been found in different compounds [13,34–36]. For the hole-doped $La_{1.905}Ba_{0.095}CuO_4$ superconductor, it is suggested that the intense pump pulse could drive the out-of-plane apical oxygens to deviate from their equilibrium positions, resulting in a modulation of Cu-apical oxygen bond lengths between different CuO_2 planes, and therefore two different Josephson coupling strengths [20]. For the electron-doped cuprate, the Cu is strictly square-planar coordinated with no apical oxygen, as shown in Fig. 4(a). Even if we assume that the pump can drive the oxygen at the $(0, 1/2, 1/4)$ position to deviate from its equilibrium position either downward or upward, it still cannot result in inequivalent coupling strengths between neighboring two CuO_2 planes in the T' structure as displayed in Fig. 4(b). This is very different from the T structure of hole-doped cuprates with the presence of apical oxygens. To obtain a modulation of different coupling strengths, we have to assume that the CuO_2 planes would be affected by the intense pump [37]. Like the T structure of hole-doped cuprate, the T' structure also has a body-centered-tetragonal structure which can be considered as two subtetragonal lattices shifting relatively with a wave vector of $(1/2, 1/2, 1/2)$ in real space. If we assume that the intense pump can cause two subtetragonal lattices to have a small displacement along the c axis relative to the static state, then

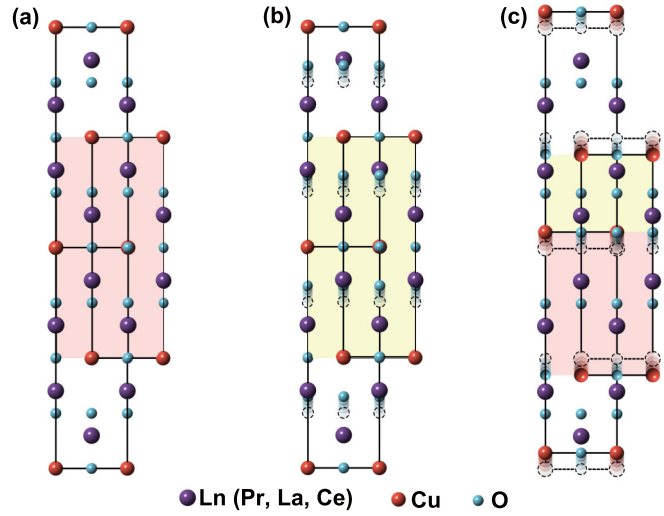

FIG. 4. A possible scenario for the presence of inequivalent coupling strength between different CuO_2 planes. (a) Electron-doped HTSC is characterized by a lack of apical oxygens, which are always related to photoexcitation induced phase transition in hole-doped HTSC. (b) Inequivalent coupling strengths can not be obtained by the deviation of oxygen at $(0, 1/2, 1/4)$ position from its equilibrium position. (c) Two different Josephson coupling strengths (shaded in different colors) can be induced by speculating the displacement of two subtetragonal lattices.

the spacing modulation between neighboring CuO_2 planes could develop, as illustrated in Fig. 4(c). As a result, two different Josephson coupling strengths could be induced. This would explain the formation of two longitudinal Josephson plasmons and a transverse mode. At present, this is purely a speculation. Apparently, further detailed studies on the photoinduced structural change and its decay dynamics by other time-resolved probes below T_c are needed to verify this scenario.

The measurement results may shed light in understanding the photoinduced phase-transition phenomena in cuprates and other strongly correlated materials. A leading interpretation for the photoinduced phase-transition phenomena in cuprates and related materials is so-called phonon pumping [15–17]. Key to those experiments is the resonant pumping of the relevant infrared active CuO mode being associated with either the apical oxygen or oxygen within CuO_2 plane. Since the pumping energy at about 1 eV in the present study is much higher than the highest CuO phonon mode (which is lower than 0.1 eV), resonant phonon pumping is unambiguously ruled out. Nevertheless, the significant photoinduced effect revealed in this work indicates that the NIR pumping can also lead to distortion or displacement of the lattice structure through nonlinear photonics.

To summarize, we performed NIR pump, c-axis THz probe measurement on a superconducting single-crystal PLCCO with $T_c = 22$ K. The intense pump induces a splitting of Josephson plasma edge below T_c. The photoexcitation induced spectral change does not exhibit observable decay up to the longest measured time delay 210 ps. With increasing the pump fluence, the splitting effect gets more significant. The measurement reveals that intense NIR pump drives the system

from an equilibrium superconducting state with uniform Josephson coupling strength to a metastable superconducting phase with modulated Josephson coupling strengths, rather than destroying superconductivity or exciting quasiparticles to unoccupied states far above the Fermi level. We speculate that the intense near infrared pump induces certain sort of displacement of the lattice structure.

This work was supported by the National Science Foundation of China (Grants No. 11327806 and No. GZ1123) and the National Key Research and Development Program of China (Grants No. 2016YFA0300902, No. 2017YFA0302903, No. 2017YFA0302904). P.C.D. was supported by the U.S. DOE, BES under Contract No. DE-SC0012311 and the Robert A. Welch Foundation Grant No. C-1839.

[1] Y. Tokura, H. Takagi, and S. Uchida, Nature (London) **337**, 345 (1989).
[2] H. Takagi, S. Uchida, and Y. Tokura, Phys. Rev. Lett. **62**, 1197 (1989).
[3] N. P. Armitage, P. Fournier, and R. L. Greene, Rev. Mod. Phys. **82**, 2421 (2010).
[4] C. Giannetti, M. Capone, D. Fausti, M. Fabrizio, F. Parmigiani, and D. Mihailovic, Adv. Phys. **65**, 58 (2016).
[5] Y. Liu, J. F. Whitaker, C. Uher, J. Peng, Z. Y. Li, and R. L. Greene, Appl. Phys. Lett. **63**, 979 (1993).
[6] Y. Long, L. Zhao, B. Zhao, X. Qiu, C. Zhang, P. Fu, L. Wang, Z. Zhang, S. Zhao, Q. Yang, and G. Wang, Physica C (Amsterdam) **436**, 59 (2006).
[7] N. Cao, Y. Long, Z. Zhang, J. Yuan, L. Gao, B. Zhao, S. Zhao, Q. Yang, J. Zhao, and P. Fu, Physica C (Amsterdam) **468**, 894 (2008).
[8] J. P. Hinton, J. D. Koralek, G. Yu, E. M. Motoyama, Y. M. Lu, A. Vishwanath, M. Greven, and J. Orenstein, Phys. Rev. Lett. **110**, 217002 (2013).
[9] I. M. Vishik, F. Mahmood, Z. Alpichshev, N. Gedik, J. Higgins, and R. L. Greene, Phys. Rev. B **95**, 115125 (2017).
[10] M. Beck, M. Klammer, I. Rousseau, M. Obergfell, P. Leiderer, M. Helm, V. V. Kabanov, I. Diamant, A. Rabinowicz, Y. Dagan, and J. Demsar, Phys. Rev. B **95**, 085106 (2017).
[11] A. Rothwarf and B. N. Taylor, Phys. Rev. Lett. **19**, 27 (1967).
[12] L. Stojchevska, I. Vaskivskyi, T. Mertelj, P. Kusar, D. Svetin, S. Brazovskii, and D. Mihailovic, Science **344**, 177 (2014).
[13] N. Gedik, D.-S. Yang, G. Logvenov, I. Bozovic, and A. H. Zewail, Science **316**, 425 (2007).
[14] K. W. Kim, A. Pashkin, H. Schafer, M. Beyer, M. Porer, T. Wolf, C. Bernhard, J. Demsar, R. Huber, and A. Leitenstorfer, Nat. Mater. **11**, 497 (2012).
[15] D. Fausti, R. I. Tobey, N. Dean, S. Kaiser, A. Dienst, M. C. Hoffmann, S. Pyon, T. Takayama, H. Takagi, and A. Cavalleri, Science **331**, 189 (2011).
[16] S. Kaiser, C. R. Hunt, D. Nicoletti, W. Hu, I. Gierz, H. Y. Liu, M. Le Tacon, T. Loew, D. Haug, B. Keimer, and A. Cavalleri, Phys. Rev. B **89**, 184516 (2014).
[17] W. Hu, S. Kaiser, D. Nicoletti, C. R. Hunt, I. Gierz, M. C. Hoffmann, M. Le Tacon, T. Loew, B. Keimer, and A. Cavalleri, Nat. Mater. **13**, 705 (2014).
[18] D. Nicoletti, E. Casandruc, Y. Laplace, V. Khanna, C. R. Hunt, S. Kaiser, S. S. Dhesi, G. D. Gu, J. P. Hill, and A. Cavalleri, Phys. Rev. B **90**, 100503(R) (2014).
[19] E. Casandruc, D. Nicoletti, S. Rajasekaran, Y. Laplace, V. Khanna, G. D. Gu, J. P. Hill, and A. Cavalleri, Phys. Rev. B **91**, 174502 (2015).
[20] S. J. Zhang, Z. X. Wang, L. Y. Shi, T. Lin, M. Y. Zhang, G. D. Gu, T. Dong, and N. L. Wang, Phys. Rev. B **98**, 020506(R) (2018).
[21] S. Li, S. Chi, J. Zhao, H.-H. Wen, M. B. Stone, J. W. Lynn, and P. Dai, Phys. Rev. B **78**, 014520 (2008).
[22] S. J. Zhang, Z. X. Wang, T. Dong, and N. L. Wang, Front. Phys. **12**, 127802 (2017).
[23] E. J. Singley, D. N. Basov, K. Kurahashi, T. Uefuji, and K. Yamada, Phys. Rev. B **64**, 224503 (2001).
[24] J. Schützmann, S. Tajima, S. Miyamoto, Y. Sato, and R. Hauff, Phys. Rev. B **52**, 13665 (1995).
[25] C. Homes, T. Timusk, D. Bonn, R. Liang, and W. Hardy, Physica C (Amsterdam) **254**, 265 (1995).
[26] E. J. Singley, M. Abo-Bakr, D. N. Basov, J. Feikes, P. Guptasarma, K. Holldack, H. W. Hübers, P. Kuske, M. C. Martin, W. B. Peatman, U. Schade, and G. Wüstefeld, Phys. Rev. B **69**, 092512 (2004).
[27] D. van der Marel and A. Tsvetkov, Czech. J. Phys. **46**, 3165 (1996).
[28] H. Shibata and T. Yamada, Phys. Rev. Lett. **81**, 3519 (1998).
[29] M. Grüninger, D. van der Marel, A. A. Tsvetkov, and A. Erb, Phys. Rev. Lett. **84**, 1575 (2000).
[30] T. Timusk and C. C. Homes, Solid State Commun. **126**, 63 (2003).
[31] S. Tajima and S. I. Uchida, Physica C (Amsterdam) **481**, 55 (2012).
[32] K. M. Kojima, S. Uchida, Y. Fudamoto, and S. Tajima, Phys. Rev. Lett. **89**, 247001 (2002).
[33] A. D. LaForge, W. J. Padilla, K. S. Burch, Z. Q. Li, S. V. Dordevic, K. Segawa, Y. Ando, and D. N. Basov, Phys. Rev. B **76**, 054524 (2007).
[34] M. Rini, R. Tobey, N. Dean, J. Itatani, Y. Tomioka, Y. Tokura, R. W. Schoenlein, and A. Cavalleri, Nature (London) **449**, 72 (2007).
[35] B. J. S. Vance R. Morrison, R. P. Chatelain, K. L. Tiwari, A. Hendaoui, A. Bruhács, and M. Chaker, Science **346**, 445 (2014).
[36] H. Ichikawa, S. Nozawa, T. Sato, A. Tomita, K. Ichiyanagi, M. Chollet, L. Guerin, N. Dean, A. Cavalleri, S.-I. Adachi, T.-H. Arima, H. Sawa, Y. Ogimoto, M. Nakamura, R. Tamaki, K. Miyano, and S.-Y. Koshihara, Nat. Mater. **10**, 101 (2011).
[37] R. Mankowsky, A. Subedi, M. Forst, S. O. Mariager, M. Chollet, H. T. Lemke, J. S. Robinson, J. M. Glownia, M. P. Minitti, A. Frano, M. Fechner, N. A. Spaldin, T. Loew, B. Keimer, A. Georges, and A. Cavalleri, Nature (London) **516**, 71 (2014).